Available online at www.sciencedirect.com
ScienceDirect
Acta Materialia 56 (2008) 4702–4714
Acta MATERIALIA
www.elsevier.com/locate/actamat

Nanoscale surficial films and a surface transition in V_2O_5–TiO_2-based ternary oxide systems

H. Qian, J. Luo *

School of Materials Science and Engineering, Center of Optical Materials Science and Engineering Technologies (COMSET), Clemson University, Clemson, SC 29634, USA

Received 3 April 2008; received in revised form 5 May 2008; accepted 16 May 2008
Available online 23 June 2008

Abstract

Nanoscale, vanadia-based, quasi-liquid films of self-selecting (equilibrium) thickness were observed on TiO_2 surfaces in six ternary oxide systems (Ti–V–X–O; X = P, Na, K, Nb, Mo or W). It is demonstrated that the film appearance and thickness could be tailored via co-doping or changing the equilibration temperature. Furthermore, the observed discontinuous changes in film thickness, hysteresis and bimodal thickness distributions indicate a first-order monolayer-to-multilayer adsorption transition, which is interpreted as a coupled prewetting and premelting transition. The film thickness and stability are measured as functions of equilibration temperature, anneal time, thermal treatment history, co-doping, overall composition and TiO_2 phase and orientation. The characterization of more than 850 independent films represents the most systematic measurement of similar interfacial films to date, providing insights into the formation mechanisms and the thermodynamic stability of equilibrium-thickness surficial films and analogous intergranular films.

Keywords: Wetting; Surface segregation; Phase transformation; Interfaces; Catalysis

1. Introduction

Nanoscale, impurity-based films of similar character have been widely observed at grain boundaries (GB) in ceramics [1–6] and metals [3,7,8], at hetero-interfaces in ceramic–ceramic [3] and metal–oxide [9–12] systems, and on free surfaces in oxides [11,13–17]. These films are called intergranular (glassy) films (IGF) or surficial amorphous films (SAF), although some partial structural order generally exists within them [3,13]. These surficial and intergranular films represent non-wetting conditions. Sufficient data are now available to interpret these IGF and SAF alternatively as equilibrium-thickness interfacial films [1,3,13,18,19] or multilayer adsorbates [2–6,13,16,19]. Nanometer-thick, impurity-based, quasi-liquid films can also be stabilized below the bulk solidus temperatures [3], where analogies to the simpler interfacial phenomena of premelting (in unary systems) [20] and prewetting (in binary de-mixed liquids) [21] can be made. Further discussions of these related interfacial phenomena and terms/jargon can be found in recent reviews [3,13].

Recently, Tang et al. [22] proposed that subsolidus IGF can be understood as quasi-liquid interfacial films formed from coupled GB prewetting and premelting transitions in a diffuse-interface model, and these GB transitions can be first order. A similar theory has also been proposed for SAF [19]. Furthermore, Dillon et al. observed several disordered GB structures (complexions) in doped Al_2O_3, implying the existence of GB transitions between them [5,6]. Yet, first-order transitions from monolayer/submonolayer adsorption to nanoscale quasi-liquid films have not been directly observed at surfaces or GB in ceramics. In addition to their scientific significance, GB and surface transitions are of practical importance because they cause abrupt changes in transport kinetics [5,6] and material properties [3]. Consequently, this study sought a surface transition in V_2O_5–TiO_2-based systems.

* Corresponding author. Tel.: +1 864 656 5961; fax: +1 864 656 1453.
E-mail addresses: jianluo@clemson.edu, jluo@alum.edu (J. Luo).

1359-6454/$34.00
doi:10.1016/j.actamat.2008.05.027

Titania-supported vanadia (V_2O_5/TiO_2) catalysts are widely used for partial oxidation and ammoxidation of alkylaromatic compounds and selective catalytic reduction of NO_x [23–28]. Furthermore, V_2O_5/TiO_2 is a model system for a broad class of "monolayer catalysts", including MoO_3/Al_2O_3, CrO_3/Al_2O_3, WO_3/Al_2O_3, Re_2O_7/Al_2O_3, TiO_2/SiO_2, Fe_2O_3/SiO_2, NiO/ZrO_2 and WO_3/ZrO_2 [23,25,29]. It is generally believed that monolayer surface adsorption of the catalytic oxide species on refractory oxide supports occurs during calcination (isothermal annealing) in these systems. This thermal spreading occurs at ~350–450 °C for V_2O_5/TiO_2 [24,25]. However, nanoscale, amorphous films are occasionally observed in V_2O_5/TiO_2, and the thickness of these films is assumed to be supply controlled [27,28]. It is further suggested that these amorphous films form owing to an unknown impurity effect [24]. A recent letter [17] reported the stabilization of nanoscale quasi-liquid films for V_2O_5 on TiO_2 anatase (1 0 1) facets at moderate (yet subeutectic) temperatures of ~550–600 °C, using purer (99.7+%) anatase powder (as opposed to the ~99% pure pigment grade powders used in the prior study [28] and in industry). Upon achieving thermodynamic equilibrium, these surficial films exhibit an equilibrium thickness independent of synthesis routes, annealing time and the amount of excess secondary phases [17]. In the present study, the impurity effects (using 99.99% anatase powder plus controlled co-doping) and the films formed on different facets and curved surfaces were further investigated. Moreover, the concept of controlling the film appearance and thickness thermodynamically via co-doping or temperature was exploited, which is of practical importance in tailoring supported oxide catalysts and controlling SAF of self-selecting thickness for other applications (e.g., device junctions or morphological control of nanocrystals) [13].

This study was further motivated by the critical need to develop a systematic dataset to probe the formation mechanisms of SAF and analogous IGF. Nanometer-thick IGF, ubiquitous in structural ceramics, thick-film resistors, varistors, high T_c superconductors and refractory metals, are known to play important roles in sintering and grain growth, and in the mechanical and physical properties of these materials (see, e.g., a recent review article [3] and references therein). However, the much needed systematic measurements of temperature- and composition-dependent IGF stability are lacking owing to the low efficiency of TEM specimen preparation and the complexity of controlling GB crystallography, whereas systematic measurements of analogous SAF on a fixed surface orientation are feasible via a more efficient powder experiment [13]. Such measurements can reveal the SAF formation mechanism, which is of critical importance; furthermore, they can provide insights into the understanding of parallel IGF, for which collecting large amounts of data is difficult. In addition, because V_2O_5/TiO_2 particles are relatively stable against coarsening, SAF are observed more frequently in V_2O_5/TiO_2 than in the Bi_2O_3/ZnO model system [13,15,16]. This permits even more systematic measurements of the film appearance and thickness as a function of various experimental parameters. These measurements were then used to test key hypotheses on the thermodynamic stability and formation mechanisms of SAF and analogous IGF, which was the purpose of this study.

2. Experimental procedure and data analysis

TiO_2 anatase particles (5–15 nm, 99.99%, the purest nano-sized anatase particles commercially available) were purchased from MTI Corporation (Richmond, CA) and annealed at 250 °C for 4 h to remove moisture. Nano-sized rutile particles were purchased from Sigma-Aldrich. Ammonium vanadate precursor (NH_4VO_3, 99.995%) was purchased from Alfa Aesar. Mixtures of TiO_2 particles and vanadate precursor were prepared by incipient wetness impregnation in aqueous solutions [28]. The mixtures were dried at 85 °C overnight, and an additional cycle of wet impregnation and drying was used to add co-dopants. Here, a co-dopant is defined as a cationic additive other than Ti and V. Co-dopants of Mo, W, Nb, K, Na and P were introduced via using the following precursors: $(NH_4)_2MoO_4$ (99.997%; Alfa Aesar), $(NH_4)_2WO_4$ (99.99+%; Alfa Aesar), $Nb(HC_2O_4)_5 6H_2O$ (Alfa Aesar), K_2CO_3 (99.995+%; ACROS), Na_2CO_3 (99.98+%; Fisher), and H_3PO_4 (99.95+%; Alfa Aesar). The dried specimens were annealed at 220 °C for 3 h and calcined at 450 °C (or 350 °C for selected P co-doped specimens to reduce P_2O_5 evaporation) for 3 h in open containers to form binary or ternary oxides (although a small fraction of carbonates was expected to remain in the specimens that were co-doped with Na and K). Finally, the oxide mixtures were isothermally annealed at the desired equilibration temperatures in closed containers and then air quenched. Specimens were isothermally annealed at each desired temperature for 4 h unless otherwise noted.

X-ray diffraction (XRD) experiments were carried out using a Scintag 2000 diffractometer (Cu K_α radiation, $\lambda = 1.5418$ Å, operating at 40 kV and 35 mA). High-resolution transmission electron microscopy (HRTEM) specimens were prepared by dispersing particles ultrasonically in acetone and placing a small amount of suspension onto carbon-coated Cu grids. The specimens were then dried overnight in a desiccator. Particle surfaces were characterized using a Hitachi 9500 microscope (300 kV, LaB_6 source, 0.10 nm lattice resolution and 0.18 nm point-to-point resolution). Minimum exposure was used during HRTEM to avoid electron beam damage. For statistical analysis, images of randomly selected particle surfaces were recorded. Scale bars were calibrated prior to measurements of film thickness.

To ensure that specimens had the proper "edge-on" conditions to measure film thickness accurately, for films on (1 0 1) or (0 0 1) facets, HRTEM images were used only if the parallel (1 0 1) or (0 0 1) fringes were clearly imaged so that the electron beam was parallel to the surfaces, thus

ensuring that the corresponding errors in thickness measurements were small. For films on curved surfaces, such errors are generally insignificant. Furthermore, these errors in measured thicknesses should be no greater than the typical surface-to-surface variations in measured film thicknesses. The standard deviations of measured thicknesses were ~0.15 nm for films without co-doping (Table 1), being close the point-to-point resolution of the microscope (0.18 nm). Thus, the effects of misalignment on film thickness measurements were relatively insignificant.

To measure the film thickness, two lines were drawn to represent the dividing planes for the crystal–film and film–vapor interfaces, respectively. Examples are shown in Fig. 1. When small crystallites or partial order were observed within the film, the dividing line for the crystal–film interface was assumed to be the outmost continuous line in the crystal (thus the small crystallites were in the film). An example is shown in Fig. 1b.

The measured film thicknesses were averaged twice for each specimen. First, film thickness was measured at every 4 nm along the surface for each independent SAF. The mean of these measurements represents the thickness of one independent SAF, and the corresponding standard deviation (σ_u) represents the film uniformity. Next, the mean thicknesses of multiple independent films were again averaged. The corresponding standard deviation (σ) represents a surface-to-surface variation in the thickness of films on different particle surfaces in one specimen. In Table 1, n

Table 1
Summary of measurements of SAF in V_2O_5–TiO_2-based systems

Specimens	(1 0 1) facets		Curved		(0 0 1) facets		Notes
	$\mu \pm \sigma$ (nm)	$n + (n_2)$	$\mu \pm \sigma$ (nm)	$n/(n_2)$	$\mu \pm \sigma$ (nm)	$n + (n_2)$	
(1.2–14.7)Ti:1V, 600 °C (2–24 h)	1.11 ± 0.25	109					[a,b]
5.2Ti:1V, 600 °C	0.97 ± 0.21	7					[a]
5.2Ti:1V, 575 °C	0.78 ± 0.13	8					[a]
5.2Ti:1V, 550 °C	0.71 ± 0.12	5					[a]
5.2Ti:1V, 500 °C	0.00	(6)					[a]
5.2Ti:1V, 600 °C + 550 °C	0.56 ± 0.09	7					[a]
5.2Ti:1V, 600 °C + 500 °C	0.47 ± 0.06	7					[a]
5.2Ti:1V,600 °C + 450 °C	0.00	(8)					[a]
3.1Ti:1V, 600 °C	0.94 ± 0.12	18	0.69 ± 0.12	11	0.00	(2)	
5.2Ti:1V, 600 °C	0.97 ± 0.15	56	0.79 ± 0.20	29	0.89 ± 0.03	5 + (3)	
8.1Ti:1V, 600 °C	0.92 ± 0.21	10					
14.6Ti:1V, 600 °C	0.61 ± 0.12	15					[c]
5.2Ti:1V, 600 °C (2 h)	0.82 ± 0.10	7					[c]
5.2Ti:1V, 550 °C	0.63 ± 0.06	10					
5.2Ti:1V:0.07P, 600 °C	0.94 ± 0.22	32	0.80 ± 0.16	8	0.77 ± 0.02	2	
5.2Ti:1V:0.1P, 600 °C	1.10 ± 0.21	123	1.05 ± 0.31	24	1.12 ± 0.13	2	
5.2Ti:1V:0.2P, 600 °C	1.22 ± 0.34	42	1.14 ± 0.18	5			
5.2Ti:1V:0.4P, 600 °C	0.97 ± 0.16	20	1.00 ± 0.17	9			
5.2Ti:1V:1P, 600 °C	1.15 ± 0.23	17					
9.2Ti:1V:0.1P, 550 °C	0.99 ± 0.21	12	0.92 ± 0.09	2	0.86	1	
5.2Ti:1V:0.1P, 550 °C	1.20 ± 0.31	19	1.35 ± 0.33	6			
5.2Ti:1V:0.1P, 525 °C	0.93 ± 0.13	5	1.10 ± 0.14	5			
5.2Ti:1V:0.1P, 500 °C	0.00	(7)	0.00	(5)			
5.2Ti:1V:0.1P, 550 °C + 500 °C	0.95 ± 0.20	11	1.31 ± 0.37	2			
5.2Ti:1V:0.1P, 550 °C + 450 °C	0.45 ± 0.30	20 + (4)	0.47 ± 0.09	9	0.62	1	
5.2Ti:1V:0.1P, 550 °C + 450 °C (24 h)	~0.00	1 + (25)	0.00	(5)			
5.2Ti:1V:0.1P, 550 °C + 400 °C	0.16 ± 0.25	9 + (20)	0.00	(3)	0.00	(1)	
5.2Ti:1V:0.1Na, 600 °C	1.00 ± 0.14	14	1.14	1	0.00	(1)	
5.2Ti:1V:0.1K, 600 °C	0.99 ± 0.08	14					
5.2Ti:1V:0.1Mo, 600 °C	0.76 ± 0.15	16	0.53	1	0.79	1	
5.2Ti:1V:0.2Mo, 600 °C	0.62 ± 0.10	24					
5.2Ti:1V:0.1W, 600 °C	0.76 ± 0.10	32	0.84 ± 0.21	6			
5.2Ti:1V:0.12W, 600 °C	0.61 ± 0.06	18					
5.2Ti:1V:0.2W, 600 °C	0.55 ± 0.08	9					
5.2Ti:1V:1W, 600 °C	0.64 ± 0.17	20					
5.2Ti:1V:0.1Nb, 600 °C	0.82 ± 0.13	13					
5.2Ti:1V:0.2Nb, 600 °C	0.72 ± 0.17	8					

Here, μ and σ are the mean and the standard deviation, respectively, of the thicknesses of measured films, n is the number of independent films observed, and n_2 is the number of surfaces that are devoid of films. Anneal time was 4 h at each temperature unless otherwise noted in parentheses. For curved surfaces, surfaces that are devoid of films are not included for computing μ and σ, except that the thicknesses were noted as zero if no films were found.

[a] Data reported in Ref. [17]. These specimens were prepared using 99.7% pure anatase powder (whereas all other specimens were prepared using 99.99% pure anatase powder).

[b] This set of data includes 15 different specimens prepared using different synthesis routes, overall nominal compositions, and annealing times. But all these 15 specimens represent V_2O_5-saturated specimens equilibrated at 600 °C [17].

[c] Film thicknesses may be limited kinetically.

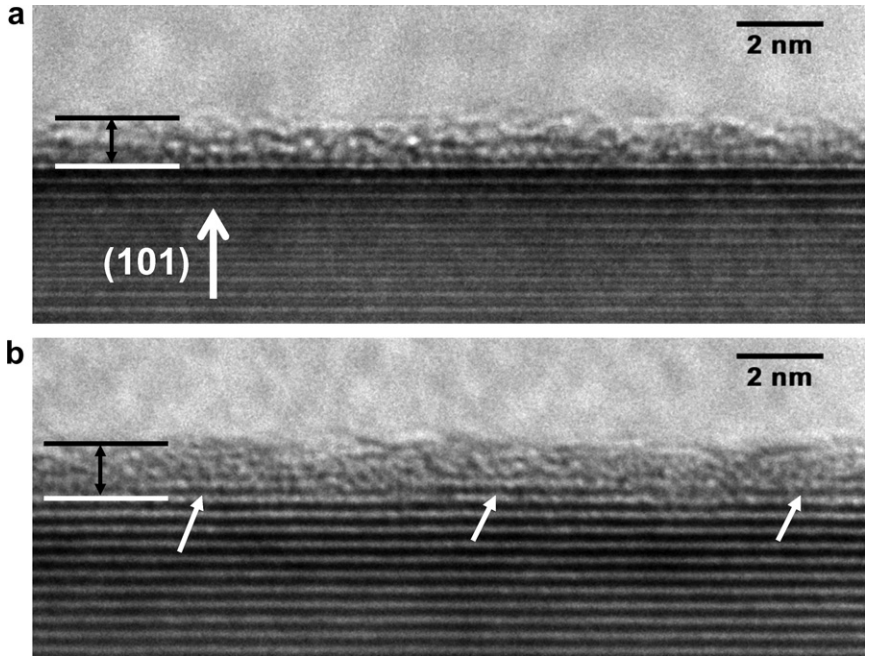

Fig. 1. Representative HRTEM images of vanadia-based SAF on (1 0 1) facets of TiO_2 anatase particles. The small epitaxial clusters, occasionally observed and presumed to have formed during cooling, are indicated by the arrows in panel (b). This is a 5.2Ti:1V specimen annealed at 600 °C for 4 h.

represents the number of independent SAF (each on a different particle surface). Approximately 1000 separate particle surfaces (including both independent SAF and surfaces without films) were characterized, and >3000 individual thickness measurements were made. Ninety-five percent confidence intervals were calculated from the standard deviations (σ) and the numbers of independent SAF (n).

Specimens were designated by the cationic ratios and normalized to 1 V. For example, "5.2Ti:1V:0.1P" represents a composition of "$5.2TiO_2 : \frac{1}{2}V_2O_5 : (0.1 \times \frac{1}{2})P_2O_5$" or "$TiO_2 + 8.7$ mol.% $V_2O_5 + 0.87$ mol.% P_2O_5". These compositions are nominal overall compositions of the specimens (not film compositions).

3. Results and discussion

3.1. Vanadia-based surficial films on anatase: film characteristics

Nanoscale, vanadia-based SAF have been observed to form on more than 850 anatase particle surfaces in the V_2O_5–TiO_2 binary system and in six V_2O_5–TiO_2-based ternary oxides (Table 1). Representative HRTEM images of two surficial films formed at 600 °C on anatase (1 0 1) facets are shown in Fig. 1. Though these films exhibited a large degree of structural disorder (Fig. 1a), partial or local order was often seen in HRTEM. In particular, growth of small epitaxial clusters was occasionally observed. An example is shown in Fig. 1b. These small crystallites often formed in a periodic array, which was probably due to a strain effect. It was also presumed that these crystallites had (largely) formed during cooling. Both diffuse-interface theories [1,22] and molecular dynamics modeling [30] suggest the existence of partial structural order within the films. However, partial order probably intensified during quenching, and some observed order might be due to HRTEM delocalization effects.

These SAF, uniform in thickness along the surface (Fig. 1), had measured thicknesses that varied little from surface to surface for a fixed set of equilibrium conditions. For example, the mean thickness of 56 independent films in a 5.2Ti:1V specimen annealed at 600 °C for 4 h was 0.97 nm, and the corresponding standard deviation (σ) of 0.15 nm described a surface-to-surface variation. Furthermore, each of these 56 measured mean thicknesses represented an average of three to seven measurements at different locations along the film. The average film uniformity was represented by $\bar{\sigma}_u$, the average of 56 individual σ_u (i.e., the standard deviation of measurements at different locations along one surface). This average film uniformity $\bar{\sigma}_u$ was 0.09 nm, which was lower than the surface-to-surface variation (σ) of 0.15 nm. A Gaussian-like distribution of all individual thickness measurements is shown in Fig. 2a. On average, the measured $\bar{\sigma}_u$ was about ~60% of the measured σ. Since some measured surface-to-surface variations in thickness may have resulted from misalignment and HRTEM imaging artifacts, the actual thickness distributions were probably tighter.

At a fixed equilibration temperature, V_2O_5-saturated specimens exhibited a constant thickness independent of the fraction of the V_2O_5 secondary phase (in the two-phase region with a constant V_2O_5 activity) once a thermodynamic equilibrium state was achieved. For example, for the nominal Ti/V ratios of 3.1, 5.2 and 8.1, the average measured film thicknesses were 0.94 nm, 0.97 nm and 0.92 nm, respectively, in specimens equilibrated at 600 °C

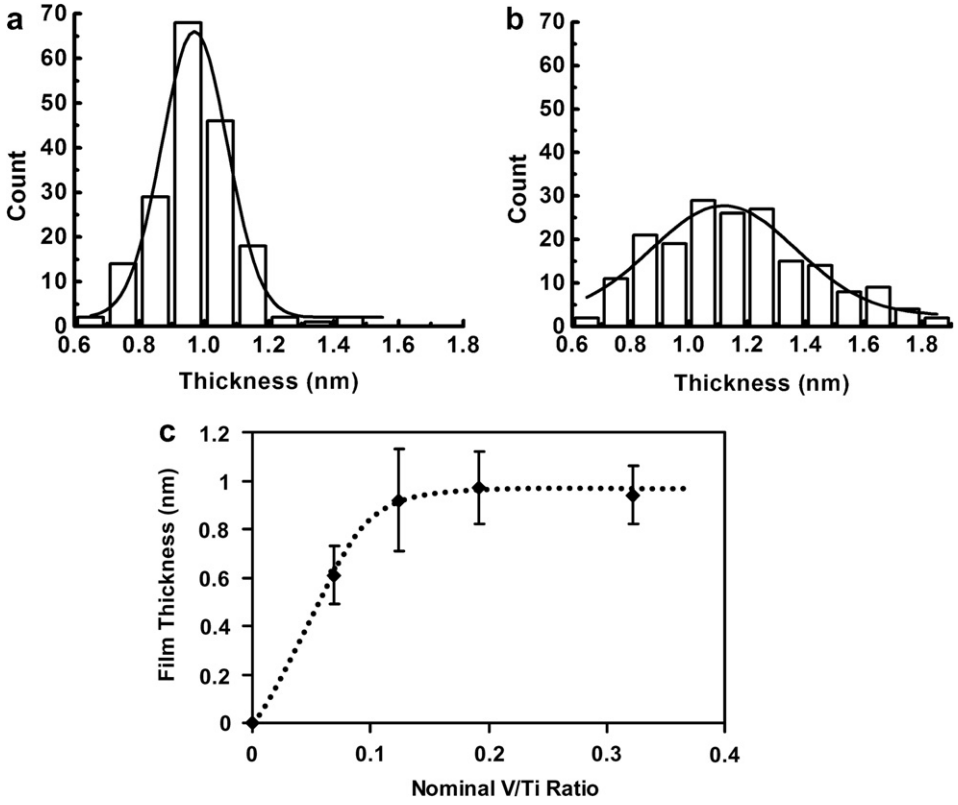

Fig. 2. Statistical distributions of measured thicknesses of films on (1 0 1) facets in (a) 5.2Ti:1V and (b) 5.2Ti:1V:0.1P specimens annealed at 600 °C for 4 h. These two distributions represent both surface-to-surface variation and film uniformity. (c) Measured average thickness vs the nominal V/Ti ratio for TiO_2–V_2O_5 binary specimens. Error bars represent standard deviations ($\pm 1\sigma$).

for 4 h (Fig. 2c). In contrast, a supply-controlled thickness, as assumed in prior studies [27,28], should strongly correlate with the overall Ti/V ratio. Consequently, this study, in which a purer anatase powder was used, confirmed the existence of equilibrium thickness [17].

The equilibrium surficial films in unsaturated specimens with V_2O_5 contents below the solid solubility limit were expected to be thinner, akin to what has been observed for Bi_2O_3-enriched surficial films on ZnO [15,16]. However, in Fig. 2c, the 14.6Ti:1V specimen probably represented a V_2O_5-saturated specimen [31], where the thickness was presumably limited by slow transport kinetics. Similarly, the films were thinner in a specimen with a shorter anneal time of 2 h (Table 1), which was also probably an effect of kinetic limitation to equilibration.

3.2. Films on surfaces of different orientations or TiO_2 phases

It is known that (1 0 1) planes are the dominant (lowest-energy) facets for anatase crystals in the Wulff shape, and (0 0 1) planes are the only other facets that are present at equilibrium [32]. The present study further confirmed that the Wulff shape for V_2O_5-doped TiO_2 anatase particles is similar. Nanoscale SAF were found on virtually all (1 0 1) facets in specimens equilibrated at temperatures of 525 °C or higher (Fig. 1; Table 1). Similar films were also observed on several (0 0 1) facets and on more than 50% of curved surfaces (Fig. 3a). For a 5.2Ti:1V specimen annealed at 600 °C for 4 h, the average measured thickness of films formed on (1 0 1) facets, (0 0 1) facets, and curved surfaces were 0.97 nm, 0.89 nm and 0.79 nm, respectively (Fig. 3b). In general, (0 0 1) facets were not frequently observed.

Vanadia-based SAF of similar character were also observed on a fraction of the surfaces in V_2O_5/rutile specimens. Measurements of five SAF on rutile (1 1 0) facets in a 5.2Ti:1V specimen annealed at 600 °C for 4 h yielded a mean thickness of 0.87 nm with a standard deviation of 0.18 nm. One SAF that was approximately 0.95 nm thick was also found on a curved rutile surface in the same specimen. This study then focused on films on anatase (1 0 1) facets and curved surfaces, which were frequently observed.

3.3. Tailoring nanoscale surficial films via co-doping

Fig. 4 shows representative HRTEM images of SAF formed on anatase (1 0 1) facets at 600 °C in 5.2Ti:1V:0.1X (X = P, Na, K, Nb, Mo or W) specimens. Small additions of co-dopants changed the film thicknesses. As shown in Fig. 5a, minor additions of the oxides of Mo, W or Nb decreased the equilibrium thickness, and films were thinner for a larger X/V ratio (0.2 vs 0.1), whereas, the addition of P increased the film thickness appreciably. The addition of K or Na had no significant effect on thickness.

The film thickness vs W/V (or P/V) ratio is shown in Fig. 5b. The film thickness initially decreased (or increased) with increasing W (or P) co-doping level, and leveled off

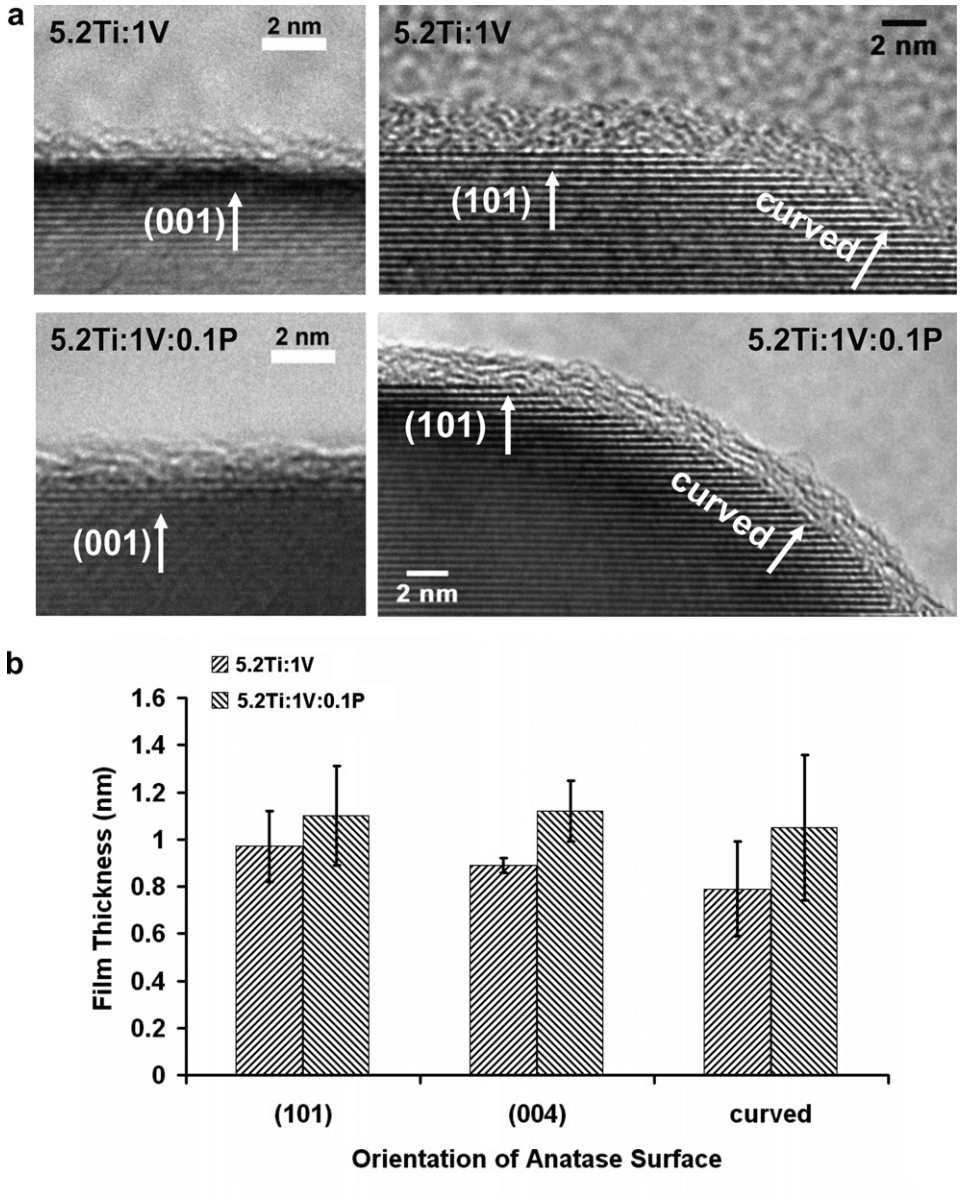

Fig. 3. (a) Representative HRTEM images of SAF on different facets and curved surfaces in 5.2Ti:1V and 5.2Ti:1V:0.1P specimens. (b) Mean thicknesses of SAF formed on anatase surfaces of different orientations. Error bars represent standard deviations ($\pm 1\sigma$). All specimens were annealed at 600 °C for 4 h.

beyond a threshold. These observations may be explained on the same basis used to explain Fig. 2c. When a relatively large amount of W (or P) was added, WO_3 (or an unknown P-enriched oxide that gave XRD peaks at $2\theta = 24.4$ and 26.9) precipitated, and the W (or P) activity leveled off. The corresponding extra XRD peaks were observable at a W/V (or P/V) ratio of ~0.1–0.2, and their intensities increased significantly when this ratio was increased to 1. This observation was consistent with the concept that equilibrium thickness depends on the chemical potential rather than on the fraction of a secondary phase.

Furthermore, co-doping also changed the thickness distribution and film appearance. As shown in Fig. 2a and Fig. 2b, adding a small amount of P (~0.87 mol.% P or a P/V ratio of 0.1) increased the average film thickness appreciably and broadened the thickness distribution. The standard deviation was approximately doubled. A comparison of film thickness variability in Fig. 2a vs Fig. 2b indicates shallow vs deep minima in corresponding free energy vs thickness curves, although the exact physical origin of this difference is unknown. Co-doping with P reduced the differences between the average thicknesses of films formed on different facets and curved surfaces (Fig. 3b). The percentage of curved surfaces covered by nanoscale SAF was ~55% for a 5.2Ti:1V specimen equilibrated at 600 °C, which increased to ~90% and >95% with the addition of 0.87 mol.% P and ~1.7 mol.% P, respectively, as shown in Fig. 6. Thus, co-doping with P resulted in thicker and more isotropic SAF, although it broadened the thickness distribution at a fixed orientation.

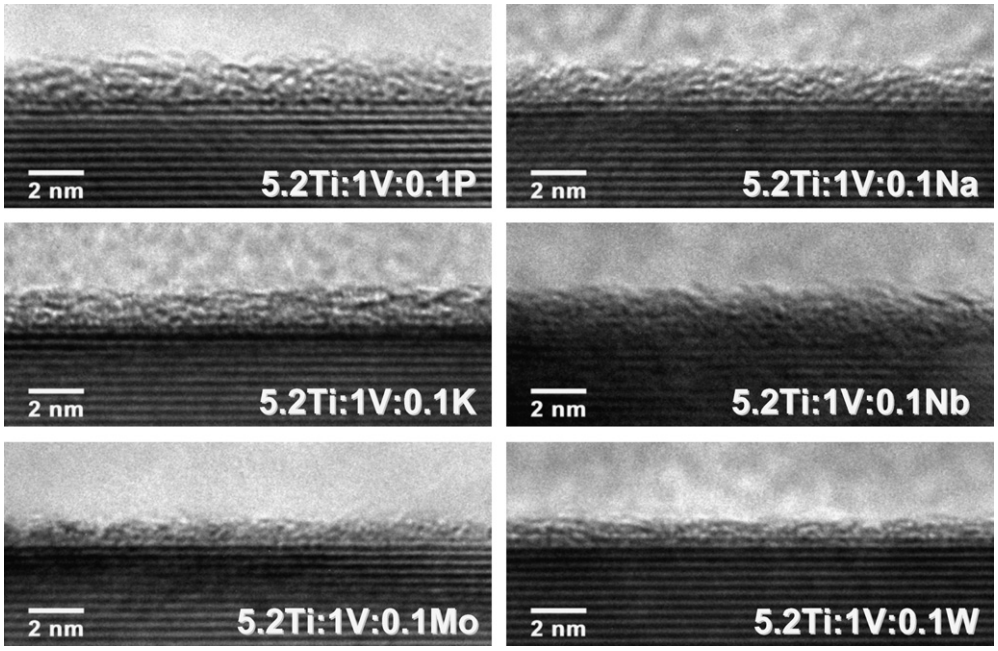

Fig. 4. Representative HRTEM images of co-doped SAF on (101) facets of anatase particles. All specimens were annealed at 600 °C for 4 h.

Determining the effects of co-doping is important for tailoring supported oxide catalysts, as industrial catalysts typically contain additives or impurities [23–28]. Tuning IGF thickness via co-doping has been reported in Si_3N_4–SiO_2-based structural ceramics with Ca [33] or rare earth [34] additives and in Pb_2RuO_7–SiO_2-based, thick-film resistors with TiO_2 additives [35]. The present study further demonstrates the concept of tailoring average SAF thickness, thickness distribution, surface coverage and anisotropy via changing the bulk chemical potentials. These observations, which support the basic theory of equilibrium-thickness SAF (and IGF), provide comprehensive data for testing thermodynamic models.

3.4. Temperature dependence of film thickness: hysteresis and bimodal distributions

The thicknesses of films formed on anatase (101) facets and curved surfaces depend on temperature, as shown in Fig. 7. To probe the kinetic limitation to equilibration, specimens were allowed to approach their equilibrium states from both lower and higher temperatures. In the first instance, 5.2Ti:1V:0.1P specimens were directly heated to the desired temperature and equilibrated for 4 h. In the second instance, specimens were annealed at 550 °C for 4 h, to elicit conditions that could form ~1.2 nm thick films [on (101) facets] or ~1.35 nm thick films (on curved surfaces). The temperature was then reduced to the equilibration temperature at which the specimens were annealed for another 4 h. At relatively low temperature ranges (~350–450 °C) in which nanoscale surficial films are not discernible by HRTEM, monolayer (or submonolayer) adsorption is known to occur based on extensive prior studies [24,25]. Upon heating, discontinuous transitions were observed from submonolayer to multilayer coverage between 500 °C and 525 °C on both (101) facets and curved surfaces (Fig. 7). Upon cooling, the transition back to submonolayer coverage occurred at somewhat lower temperatures. The transition in 5.2Ti:1V:0.1P specimens was more abrupt than that observed in the V_2O_5–TiO_2 binary system [17]. In Fig. 7a, the reported film thicknesses for specimens in which the equilibration was approached from a higher temperature (as indicated by a solid line) represent the overall average thicknesses of two groups of films (as indicated by the dotted lines).

When the equilibration was approached from a higher temperature, bimodal thickness distributions for the SAF on anatase (101) facets were observed at 400 °C and 450 °C (Fig. 8a). In a 5.2Ti:1V:0.1P specimen annealed at 550 °C × 4 h+450 °C × 4 h, SAF were observed in 16 of 20 facets (80%) of (101) orientation with an average thickness of 0.57 nm, with four (101) facets (20%) devoid of discernible films (dried). With a reduction in temperature, among 29 (101) facets examined in a specimen annealed at 550 °C × 4 h+400 °C × 4 h, SAF were found on nine facets (31%) with an average thickness of 0.55 nm, with 20 facets (69%) dried. Furthermore, an increase in the equilibration time to 24 h at 450 °C (550 °C × 4 h+450 °C × 24 h) showed that 25 of 26 (101) facets (or ~96%) were dried (Fig. 8a). A representative HRTEM image of these dried surfaces is shown in Fig. 8b.

Nanoscale SAF were observed on all (101) facets in specimens equilibrated at 525 °C and higher temperatures, as well as in one specimen fired at 550 °C × 4 h+500 °C × 4 h. As SAF only formed on a fraction of curved surfaces, the data in Fig. 7b exclude surfaces devoid of films, but the

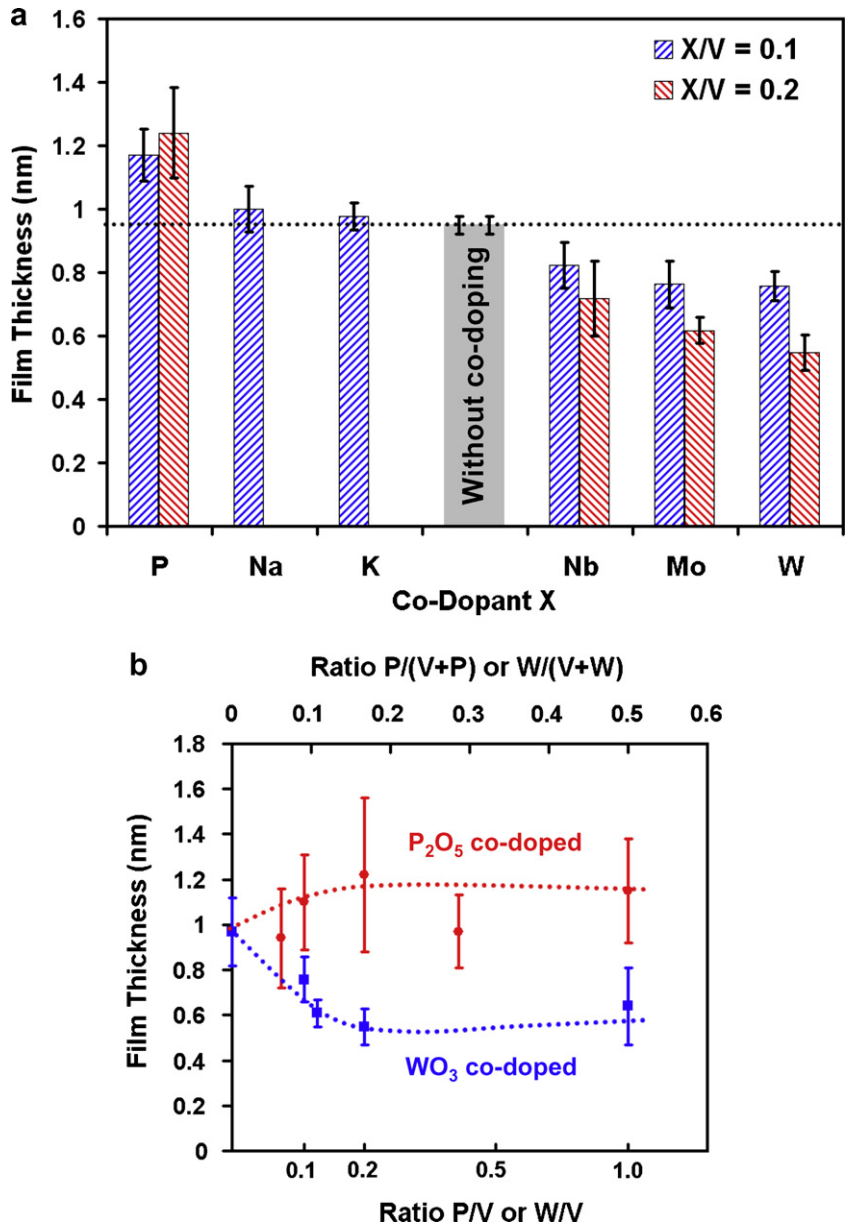

Fig. 5. (a) Effect of co-doping on mean thicknesses of SAF on (101) facets of anatase particles. (b) Film thickness vs co-doping ratio for P and W co-doped specimens. The Ti/V ratio was kept at 5.2, and all specimens were annealed at 600 °C for 4 h. In panel (b), relatively lower measured thicknesses for 5.2Ti:1V:0.07P and 5.2Ti:1V:0.4P specimens might be related to evaporative losses of P_2O_5 during calcination at 450 °C in open containers. The other three specimens co-doped with P_2O_5 were re-examined using a lower calcination temperature of 350 °C to reduce P_2O_5 loss. Panel (a) shows error bars representing 95% confidence intervals, and panel (b) shows error bars representing standard deviations ($\pm 1\sigma$).

thickness is plotted as zero in cases where no SAF were found.

These observed discontinuous changes in thickness, hysteresis and bimodal thickness distributions suggest a first-order surface adsorption transition, which will be discussed further in Section 3.7.

3.5. Films coexisting with nano-drops: an analogy to frustrated-complete wetting

Whereas nanometer-thick SAF were found to coexist with nanoscale partial-wetting glassy droplets (Fig. 9) in the same set of specimens, they were found only in a small fraction of surfaces. Similar nanoscale wetting configurations have been previously reported for Bi_2O_3 on ZnO and MoO_3 on Al_2O_3 [16]. Here, phenomenological similarities to frustrated-complete wetting [36] and pseudo-partial wetting [37,38], proposed and confirmed for molecular substances and metallic systems, clearly exist. A discussion of these analogous wetting phenomena is in Ref. [3]. Although the cooling effects are unknown, Fig. 9 indicates that the excess glassy phase did not completely wet the surfaces; thus, these surficial films exhibited a self-limiting (equilibrium) thickness.

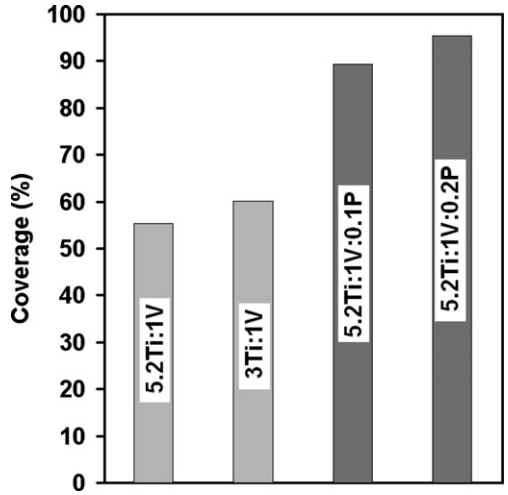

Fig. 6. Percentage of curved surfaces on which nanoscale SAF were observed. Specimen compositions are labeled. All specimens were annealed at 600 °C for 4 h. HRTEM images of randomly selected particle surfaces were recorded and used for statistical analysis.

3.6. Film stability in a phenomenological model

In a phenomenological model [13], the excess free energy of an SAF of thickness h is given by

$$G^{x}(h) = \gamma_{cl} + \gamma_{lv} + \Delta G_{vol} \cdot h + \sigma_{interfacial}(h) \quad (1)$$

where $\gamma_{cl} + \gamma_{lv}$ is the sum of crystal–liquid and liquid–vapor interfacial energies. The term ΔG_{vol} is the volumetric free energy for forming a hypothesized uniform liquid film from a mixture of bulk phases:

$$\Delta G_{vol} = \left(G^{f}_{liquid} - \sum_{i} X_i \mu_i \right) \cdot \rho \quad (2)$$

where G^{f}_{liquid} is the liquid formation free energy, X_i is average fraction of the ith component in the film, μ_i is a chemical potential of the ith component set by the (equilibrium or metastable) bulk phases, and ρ is density. This volumetric free energy is positive for quasi-liquid films equilibrated at subsolidus temperatures, and it can be evaluated via computational thermodynamics if relevant thermodynamic functions are known [39]. The $\Delta G_{vol} \cdot h$ term is generally the dominant attractive interaction in subsolidus regions that limits the film thickness [13]. Eq. (2) also implies that film thickness should depend on the chemical potentials of the bulk phases rather than the nominal overall composition or the fraction of a secondary phase, as shown in Figs. 2c and 5b.

When the film is thin, an extra interfacial free energy term $\sigma_{interfacial}(h)$ arises, representing the total contribution of all interfacial forces [13]. For SAF in oxides, this term can be expressed as

$$\sigma_{interfacial}(h) = \frac{-A_{123}}{12\pi h^2} + \sigma_{short\text{-}range}(h) + \sigma_{elec}(h) + \cdots \quad (3)$$

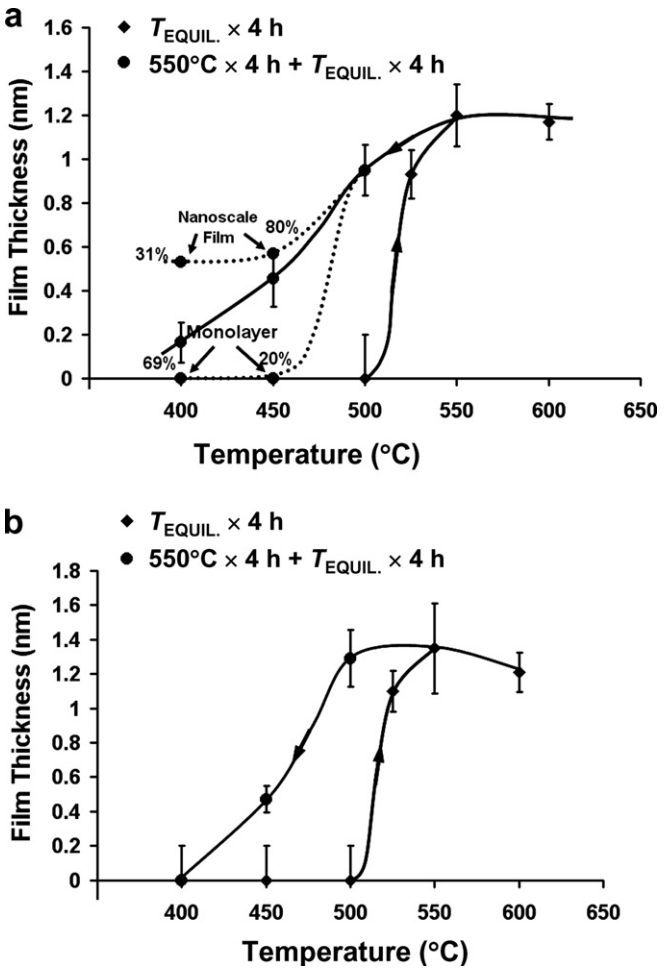

Fig. 7. Mean film thickness vs temperature for SAF formed on (a) (1 0 1) facets and (b) curved surfaces of anatase particles in 5.2Ti:1V:0.1P specimens. Measurements from two sets of specimens are reported. In the first set, specimens were directly heated to the desired temperature and equilibrated for 4 h. In the second set, specimens were first annealed at 550 °C for 4 h, and the temperature was lowered to the equilibration temperature at which the specimens were annealed for another 4 h. For specimens where equilibration was approached from a higher temperature, bimodal thickness distributions (indicated by the dotted lines and explained in Fig. 8) were observed, and the solid line represents the overall average thicknesses. HRTEM was unable to discern individual film $<\sim$0.2 nm thick. Error bars represent 95% confidence intervals and are set to be 0.2 nm for surfaces devoid of films.

The first term is a long-range London dispersion interaction. The Hamaker constant A_{123} was estimated for the V_2O_5 on anatase system from the optical and static dielectric constants of anatase ($n = 2.57$, $\varepsilon \approx 86$) [40] and V_2O_5 ($n = 1.97$–2.12, $\varepsilon \approx 20.1$–37.2, depending on orientation) [41] to be between -88 zJ and -106 zJ [42]. While this newer assessment will replace the prior inaccurate estimation [17], a more accurate calculation of A_{123} should use a full-spectrum method [43] and consider the exact V valence states and film structure (which are currently unknown). Nonetheless, this estimation suggests that the dispersion force favors complete wetting. Thus, the film thickness is probably limited by the $\Delta G_{vol} \cdot h$ term at the subsolidus regime (Fig. 10) [13,15]. In Eq. (3), $\sigma_{short\text{-}range}(h)$

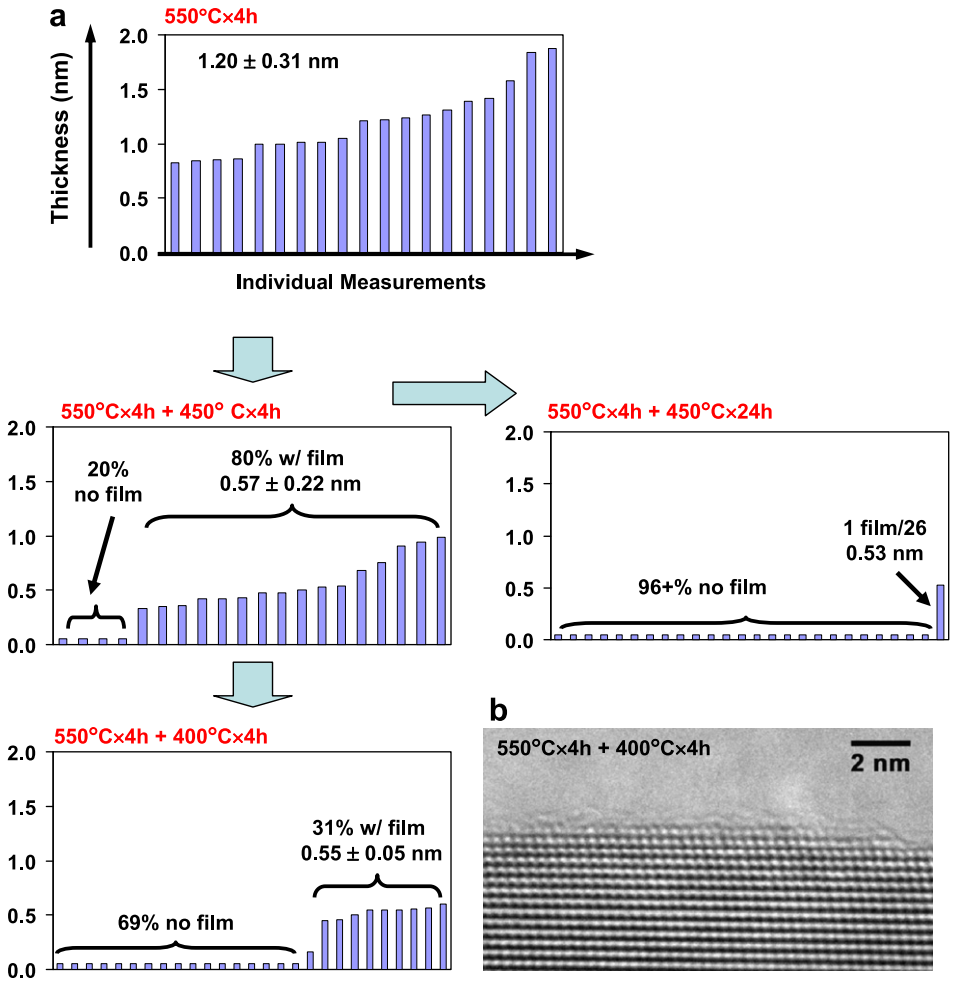

Fig. 8. (a) Evolution of bimodal distributions of measured film thicknesses for SAF formed on anatase (1 0 1) facets when equilibration was approached from a higher temperature. Each bar represents a measured thickness of an independent film on a separate particle surface. (b) A representative HRTEM image of a dried (1 0 1) facet in a 5.2Ti:1V:0.1P specimen annealed at 550 °C × 4 h+400 °C × 4 h. See text for details.

is a coupled short-range interaction of structural and chemical origins, and $\sigma_{\text{elec}}(h)$ is an electrostatic interaction. By selecting the state of $h = +\infty$ as a reference state, the free energy terms that represent interfacial forces (i.e., $\sigma_{\text{vdW}}(h)$, $\sigma_{\text{short-range}}(h)$, $\sigma_{\text{elec}}(h)$, etc., but not $\Delta G_{\text{vol}} \cdot h$) can be consistently defined so that they all vanish as $h \to +\infty$.

The excess film free energy, referred to the chemical potentials set by the bulk phases and the state of $h = 0$, is given by

$$\begin{aligned}\Delta\sigma(h) &\equiv G^{x}(h) - \gamma_{\text{cv}}^{(0)} \\ &= \Delta\gamma^{(0)} + \Delta G_{\text{vol}} \cdot h + \frac{-A_{123}}{12\pi h^2} + \sigma_{\text{short-range}}(h) \\ &\quad + \sigma_{\text{elec}}(h) + \cdots \end{aligned} \tag{4}$$

Here, $\Delta\gamma^{(0)} \equiv \left(\gamma_{\text{lv}} + \gamma_{\text{cl}} - \gamma_{\text{cv}}^{(0)}\right)$, where $\gamma_{\text{cv}}^{(0)}$ is the excess free energy of a "clean" surface without any adsorption (which defers from the true equilibrium γ_{cv} that corresponds to the global minimum in Eq. (1)). Eq. (4) is a free-surface counterpart to the Clarke model for IGF [1,18], and can be considered a high-temperature colloidal theory with an additional $\Delta G_{\text{vol}} \cdot h$ term. An "equilibrium" thickness corresponds to a global or local minimum in excess film free energy vs thickness, which is defined by:

$$\left.\frac{\mathrm{d}[\Delta\sigma(h)]}{\mathrm{d}h}\right|_{h=h_{\text{eq.}}} = 0 \tag{5}$$

These quasi-liquid surficial films probably formed at subsolidus temperatures [17,31]. A prior study, reporting a eutectic reaction in the TiO_2–V_2O_5 binary system (producing V_2O_5 and rutile) at ~631 °C [31], also suggests that a V_2O_5-induced anatase-to-rutile transition starts at ~525 °C. However, XRD analysis showed a stability of the nano-sized anatase phase in these systems for annealing up to 600 °C, in which only a minor fraction of rutile phase formed. A subsolidus quasi-liquid SAF is thermodynamically stable if $\Delta\sigma(h) < 0$, an approximated condition for which is

$$\Delta G_{\text{vol}} \cdot h < \left[\gamma_{\text{cv}}^{(0)} - (\gamma_{\text{lv}} + \gamma_{\text{cl}})\right] \tag{6}$$

Stabilization of subsolidus quasi-liquid SAF in these binary and ternary systems has phenomenological similarities to the phenomenon of premelting in unary systems [20].

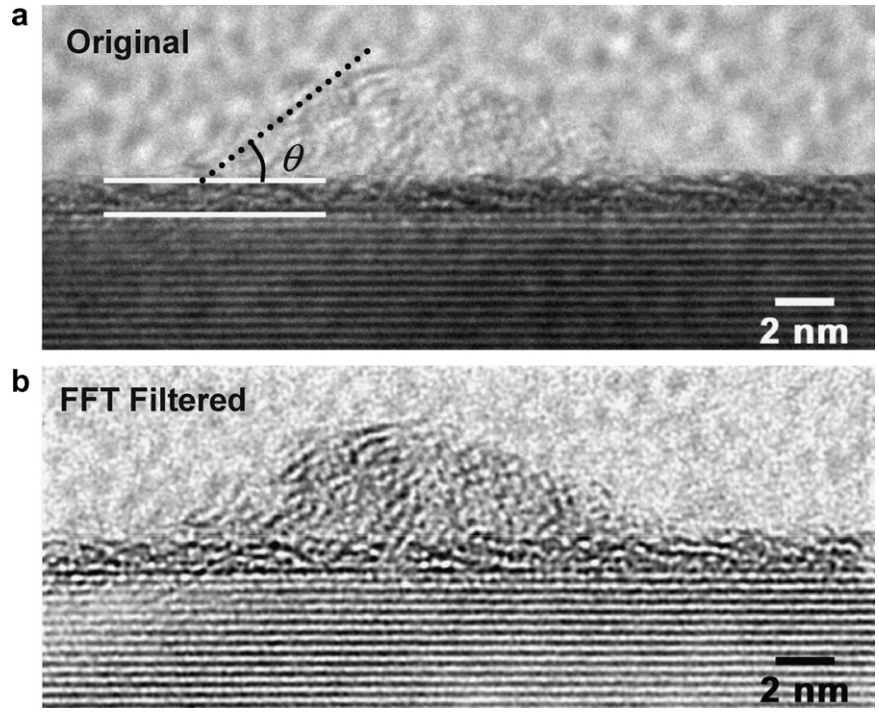

Fig. 9. (a) Original and (b) filtered HRTEM images of a nanoscale SAF coexisting with a non-wetting nano-droplet. This is a 5.2Ti:1V specimen equilibrated at 600 °C.

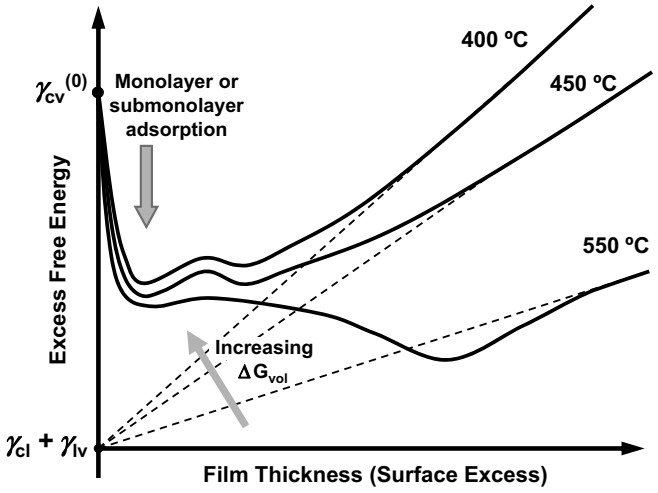

Fig. 10. Schematic illustration of proposed excess free energy vs film thickness curves. This illustration, which explains observations in Fig. 8, implies a first-order adsorption transition.

Eq. (6) illustrates that this stabilization can be conceived as if the free energy penalty for forming an undercooled liquid film is more than offset by the reduction of total interfacial energy resulting from the replacement of a high-energy "clean" crystal surface with a liquid surface and a crystal–liquid interface. In an alternative (and equivalent) approach, Eq. (4) can be rewritten as

$$\Delta\sigma(h) = \Delta\gamma^{(0)} \cdot f(h) + \Delta G_{\mathrm{vol}} \cdot h \tag{7}$$

where the interfacial coefficient $f(h) \equiv \sigma_{\mathrm{interfacial}}(h)/\Delta\gamma^{(0)} + 1$ is defined to represent the effects of all interfacial forces. By definition, $f(h)$ ranges from 0 to 1 as h increases from 0 to ∞. The $f(h)$ term can have multiple minima [44,45], leading to complex adsorption and wetting phenomena.

3.7. A first-order transition?

The observations of bimodal thickness distributions and their evolution (Fig. 8) indicate the existence of a global minimum (corresponding to monolayer or submonolayer adsorption) and a metastable minimum (corresponding to ~0.55 nm thick SAF) in excess free energy vs film thickness at 450 °C and 400 °C (Fig. 10). At higher temperatures, the global minimum is associated with nanoscale SAF. The interfacial coefficient $f(h)$ determines the specific profile of these minima and the energy barrier between them [44,45]. The switch between the global and metastable minima with changing temperature is probably triggered by the $\Delta G_{\mathrm{vol}} \cdot h$ term, which increases with a reduction of temperature in the subsolidus regime (Fig. 8). This analysis implies a first-order adsorption transition from monolayer-to-multilayer coverage, the existence of which is further supported by the observations of the hysteresis loops in the thickness vs temperature curves and the relatively abrupt transitions in film thicknesses in Fig. 7a and b.

A first-order wetting (adsorption) transition that occurs when the phase doing the wetting is not yet stable is called a prewetting transition [21]. This prewetting transition, originally proposed in the Cahn critical point wetting model for binary de-mixed liquids [46], has been observed in organic systems [47,48] and in the Pb–Ga liquid metal system [49,50]. In the present case, the transition from

low- to high-adsorption structures is coupled with an interfacial disordering transition, occurring at a subsolidus temperature, to permit an analogy to premelting in unary systems [20]. Thus, it is conceptually useful to interpret this surface transition as a coupled prewetting [46] and premelting [20] transition, which leads to the formation of quasi-liquid surficial films with a high level of adsorption. Further discussions of the phenomenological similarities among equilibrium-thickness SAF and IGF, prewetting, premelting, and frustrated-complete wetting can be found in recent review articles [3,13].

A surface transition can be modeled via a diffuse-interface theory [19], which combines the Cahn critical point wetting model for surfaces in binary de-mixed liquids [46] and the Tang–Carter–Cannon model for GB (IGF) in binary alloys [22]. In particular, the energy barrier between the two minima in the free energy vs film thickness shown in Fig. 10 is probably related to the high volumetric free energy for the intermediate state between a bulk (binary) liquid and a bulk crystal [19]. This energy barrier is the possible origin of the first-order transition. The hysteresis and bimodal thickness distributions shown in Figs. 7 and 8 are probably related to the nucleation of small crystallites in surficial films (when the mass transport rate is limited), and such crystallites can be seen in Fig. 1b.

Recent discoveries of multiple GB complexions (phases) with possible GB transitions in doped Al_2O_3 by Dillon et al. [5,6] resolves an outstanding scientific problem of the abnormal grain growth mechanism. Indications of GB prewetting/premelting transitions have also been found for Cu–Bi [51–56] and Fe–Si–Zn (where the primary phases are underlined) [53,57–60].

4. Concluding remarks

Vanadia-based, equilibrium-thickness, surficial films were observed on TiO_2 anatase (101) and (001) facets and curved surfaces in the V_2O_5–TiO_2 binary system, and in six ternary oxide systems. Co-doping can be used to tune the equilibrium thickness of these films. The average measured thickness was found to increase with the addition of P, decrease with the addition of Mo, W and Nb, and remain stable with the addition of K and Na. Co-doping can also be used to tailor the film thickness distribution, anisotropy and surface coverage. Furthermore, both film appearance and thickness can be tuned by changing equilibration temperature (and, presumably, any other intensive thermodynamic variables).

Observations of abrupt transitions in film thicknesses, hysteresis loops in the thickness vs temperature curves, and further analysis of bimodal thickness distributions and their evolution suggest the possible existence of a first-order monolayer-to-multilayer adsorption transition. Consequently, these SAF were interpreted as quasi-liquid films or multilayer adsorbates formed from coupled premelting and prewetting transitions in a generalized Cahn critical point wetting model. Since first-order surface or GB transitions can cause abrupt changes in transport kinetics (e.g., surface/GB diffusivity, GB mobility, surface reaction/growth rates) and mechanical/physical properties (e.g., creep and surface friction) [3], confirming and comprehending such transitions are important for controlling microstructural evolution, growth of nanocrystals, and properties of the resultant materials.

More than 850 independent films were observed. The measurements of film appearance and thickness as a function of various controlled parameters provide an important dataset for elucidating the general formation mechanisms of both SAF and IGF.

Further experiments to characterize the catalytic properties of these surficial films are in progress. In general, catalytic properties are probably sensitive to the detailed structure of the overlayers (i.e., monolayers or nanoscale surficial films) [61]. The specific co-doping effects probably depend on the interaction of these respective co-dopants with the dangling V=O bonds. Furthermore, the co-doping effects are expected to differ for different catalytic reactions. For selective catalytic reduction of NO_x by NH_3, MoO_3, WO_3 and Nb_2O_5 co-dopants are known as "promoters", while K_2O and Na_2O co-dopants are known to have poisoning effects [62,63]. It is also known that the addition of P_2O_5 has little effect on the catalytic activity for butadiene oxidation [62]. While there are probably no general conclusions on whether the formation of nanometer-thick surficial films and the addition of co-dopants are beneficial or detrimental on the resultant catalytic properties, the ability to tailor the structure and composition of these films via controlling thermodynamic variables offers a new dimension for tailoring supported catalysts at the nanoscale.

Acknowledgments

This research was supported by an NSF CAREER award (DMR-0448879; ceramics program). The authors thank Dr. JoAn Hudson and Amar Kumbhar for their assistance in using HRTEM, Dr. Don Vanderveer for his assistance in using XRD, and Ming Tang, Rick F. Rajter, and Dr. Roger H. French for their invaluable discussions. The authors also gratefully acknowledge the late Dr. Rowland M. Cannon Jr. for his inspiration.

References

[1] Clarke DR. J Am Ceram Soc 1987;70:15.
[2] Cannon RM, Esposito L. Z Metallkd 1999;90:1002.
[3] Luo J. Crit Rev Solid State Mater Sci 2007;32:67.
[4] Cannon RM, Rühle M, Hoffmann MJ, French RH, Gu H, Tomsia AP, et al. Adsorption and wetting mechanisms at ceramic grain boundaries. In: Sakuma T, Ikuhara Y, editors. Grain boundary engineering in ceramics, vol. 118. Westerville (OH): The American Ceramic Society; 2000. p. 427.
[5] Dillon SJ, Harmer MP. Acta Mater 2007;55:5247.
[6] Dillon SJ, Tang M, Carter WC, Harmer MP. Acta Mater 2007;55:6208.
[7] Luo J, Gupta VK, Yoon DH, Meyer HM. Appl Phys Lett 2005;87:231902.

[8] Gupta VK, Yoon DH, Meyer III HM, Luo J. Acta Mater 2007;55:3131.
[9] Avishai A, Scheu C, Kaplan WD. Acta Mater 2005;53:1559.
[10] Scheu C, Dehm G, Kaplan WD. J Am Ceram Soc 2000;84:623.
[11] Baram M, Kaplan WD. J Mater Sci 2006;41:7775.
[12] Avishai A, Kaplan WD. Acta Mater 2005;53:1571.
[13] Luo J, Chiang Y-M. Annu Rev Mater Res 2008;38, in press.
[14] Luo J, Chiang Y-M. J Eur Ceram Soc 1999;19:697.
[15] Luo J, Chiang Y-M. Acta Mater 2000;48:4501.
[16] Luo J, Chiang Y-M, Cannon RM. Langmuir 2005;21:7358.
[17] Qian H, Luo J. Appl Phys Lett 2007;91:061909.
[18] Clarke DR, Shaw TM, Philipse AP, Horn RG. J Am Ceram Soc 1993;76:1201.
[19] Luo J, Tang M, Cannon RM, Carter WC, Chiang Y-M. Mater Sci Eng A 2006;422:19.
[20] Dash JG, Rempel AM, Wettlaufer JS. Rev Mod Phys 2006;78:695.
[21] Bonn D, Ross D. Rep Prog Phys 2001;64:1085.
[22] Tang M, Carter WC, Cannon RM. Phys Rev Lett 2006;97:075502.
[23] Wachs IE, Briand LE, Jehng JM, Burcham L, Gao XT. Catal Today 2000;57:323.
[24] Wachs IE, Weckhuysen BM. Appl Catal A 1997;157:67.
[25] Xie Y-C, Tang Y-Q. Adv Catal 1990;31:1.
[26] Weckhuysen BM, Keller DE. Catal Today 2003;78:25.
[27] Centi G. Appl Catal A 1996;147:267.
[28] Sanati M, Wallenberg RL, Andersson A, Jansen S, Tu Y. J Catal 1991;132:128.
[29] Wachs IE. Catalysis 1997;13:37.
[30] Garofalini S, Luo W. J Am Ceram Soc 2003;86:1741.
[31] Habel D, Stelzer JB, Feike E, Schroder C, Hosch A, Hess C, et al. J Eur Ceram Soc 2006;26:3287.
[32] Gao W, Altman EI. Surf Sci 2006;600:2572.
[33] Tanaka I, Kleebe H-J, Cinibulk MK, Bruley J, Clarke DR, Rühle M. J Am Ceram Soc 1994;77:911.
[34] Wang C-M, Pan X, Hoffmann MJ, Cannon RM, Rühle M. J Am Ceram Soc 1996;79:788.
[35] Chiang Y-M, Silverman LA, French RH, Cannon RM. J Am Ceram Soc 1994;77:143.
[36] Bertrand E, Dobbs H, Broseta D, Indekeu J, Bonn D, Meunier J. Phys Rev Lett 2000;85:1282.
[37] Brochard-Wyart F, di Meglio J-M, Quéré D, de Gennes PG. Langmuir 1991;7:335.
[38] Moon J, Garoff S, Wynblatt P, Suter R. Langmuir 2004;20:402.
[39] Luo J, Shi X. Appl Phys Lett 2008;92:101901.
[40] Samsonov GV. The oxide handbook. New York: Plenum; 1982.
[41] Kuck S, Werheit H, editors. Landolt–Bornstein: non-tetrahedrally bonded binary compounds II. Berlin: Springer-Verlag; 2000.
[42] Israelachvili JN. Intermolecular and surface forces. London: Academic Press; 1994.
[43] French RH, Cannon RM, DeNover LK, Chiang Y-M. Solid State Ionics 1995;75:13.
[44] Dietrich S. Wetting phenomena. In: Domb C, Lebowitz JL, editors. Phase transitions and critical phenomena, vol. 12. London: Academic Press; 1988. p. 1.
[45] de Gennes PG. Rev Mod Phys 1985;57:827.
[46] Cahn JW. J Chem Phys 1977;66:3667.
[47] Kellay H, Bonn D, Meunier J. Phys Rev Lett 1993;71:2607.
[48] Schmidt JW, Moldover MR. J Chem Phys 1986;84:4563.
[49] Chatain D, Wynblatt P. Surf Sci 1996;345:85.
[50] Wynbalatt P, Chatain D. Ber Bunsenges Phys Chem 1998;102: 1142.
[51] Chang LS, Rabkin E, Straumal BB, Baretzky B, Gust W. Acta Mater 1999;47:4041.
[52] Chang L-S, Rabkin EI, Straumal B, Lejcek P, Hofmann S, Gust W. Scripta Metall Mater 1997;37:729.
[53] Straumal BB, Baretzky B. Interface Sci 2004;12:147.
[54] Straumal BB, Zieba P, Gust W. Int J Inorg Mater 2001;3:1113.
[55] Divinski S, Lohmann M, Herzig C. Acta Mater 2004;52:3973.
[56] Divinski S, Lohmann M, Herzig C, Straumal B, Baretzky B, Gust W. Phys Rev B 2005;71:104104.
[57] Straumal BB, Noskovich OI, Semenov VN, Shvindlerman LS, Gust W, Predel B. Acta Metall Mater 1992;40:795.
[58] Rabkin EI, Semenov VN, Shvindlerman LS, Straumal BB. Acta Metall Mater 1991;39:627.
[59] Noskovich OI, Rabkin EI, Semenov VN, Straumal BB, Shvindlerman LS. Acta Metall Mater 1991;39:3091.
[60] Straumal BB, Rabkin E, Lojkowski W, Gust W, Shvindlerman LS. Acta Mater 1997;45:1931.
[61] Devriendt K, Poelman H, Fiermans L. Surf Interface Anal 2000;29:139.
[62] Deo G, Wachs IE. J Catal 1994;146:335.
[63] Amiridis MD, Duevel RV, Wachs IE. Appl Catal B 1999;20:111.